

## Rupture propagation on heterogeneous fault: Challenges for predicting earthquake magnitude

杨宏峰<sup>1,2,\*</sup>, 姚素丽<sup>1</sup> and 陈翔<sup>1</sup>

Citation: [科学通报](#); doi: 10.1360/TB-2021-1086

View online: <https://engine.scichina.com/doi/10.1360/TB-2021-1086>

Published by the [《中国科学》杂志社](#)

---

### Articles you may be interested in

[Experimental studies on gas and water permeability of fault rocks from the rupture of the 2008 Wenchuan earthquake, China](#)

SCIENCE CHINA Earth Sciences **57**, 2825 (2014);

[Late Quaternary surface deformation and rupture behavior of strong earthquake on the segment north of Mianning of the Anninghe fault](#)

Science in China Series D-Earth Sciences **51**, 1224 (2008);

[Steady-state solutions of rupture propagation in an earthquake simulator governed by rate and state dependent friction](#)

European Physical Journal ST(Special Topics) **191**, 105 (2010);

[Discussion of rupture mechanisms on the seismogenic fault of the 2008  \$M\_s\$ 8.0 Wenchuan earthquake](#)

SCIENCE CHINA Earth Sciences **54**, 1360 (2011);

[The  \$M\_s\$ 7.1 Yushu earthquake surface rupture and large historical earthquakes on the Garzê-Yushu Fault](#)

Chinese Science Bulletin **55**, 3504 (2010);

---



# 非均匀断层上的破裂传播及对震级预测的挑战

杨宏峰<sup>1,2\*</sup>, 姚素丽<sup>1</sup>, 陈翔<sup>1</sup>

1. 香港中文大学地球系统科学系, 香港;
  2. 香港中文大学深圳研究院, 深圳 518057
- \* 联系人, E-mail: [hyang@cuhk.edu.hk](mailto:hyang@cuhk.edu.hk)

2021-10-22 收稿, 2022-02-25 修回, 2022-02-28 接受, 2022-03-09 网络版发表

国家重点研发计划(2018YFC1503400)、中国地震科学实验场项目(2018CSES0102)、香港研究资助局优配研究金(14306119, 14306418)和地震数值预测联合实验室开放基金(2021LNEF02)资助

**摘要** 针对发震断层上的潜在地震开展震级和地表震动预测, 对开展地震灾害区划、防震减灾等工作十分关键. 由于断裂带本身的多种非均匀性, 如断层几何、介质结构、应力的非均匀分布, 准确预测震级面临着众多挑战. 本文简要回顾了影响地震破裂传播及震级的因素, 指出了应力分布状态、断层孕震带尺度、断裂带介质结构对破裂传播过程的影响. 在非均匀应力分布下, 震级对破裂起始位置(震中)具有强烈的依赖性, 即震中-震级存在“测不准”关系, 震中对破裂是否延伸到地表也有控制作用. 走滑断裂带孕震带尺度(在倾向上的深度)对破裂是否发展为“逃逸型”大地震有控制作用. 近断裂带的介质结构对破裂方向性、延展尺度都有显著影响. 未来可通过密集地震台阵观测获取高分辨率断裂带结构, 并结合实验室流变性质测量, 推断发震断层的流变结构, 为刻画可能发震的凹凸体提供支撑. 针对震中对震级的影响, 可以通过破裂动力学模拟, 结合大地测量观测、地震学观测、实验室摩擦实验结果, 进行数值实验, 探索可能发生强震的震中区域, 为野外观测提供参照. 此外, 动力学数值模拟结果也可以弥补大地震近场地表震动观测数据缺乏的不足, 为开展基于地震物理过程的灾害区划提供参考.

**关键词** 地震预测, 断层非均匀性, 地震破裂传播, 震中依赖性, 地震动力学数值模拟

地震预测是针对未来地震的发生地点、时间、震级的定量估计, 是公认的世界性难题<sup>[1-3]</sup>. 目前, 尚无绝对可靠的预测方法, 可以在学界认可的误差范围内同时准确预测上述地震“三要素”<sup>[1]</sup>: 位置,  $\pm$ 破裂长度; 大小,  $\pm 0.5$ 破裂长度或者震级 $\pm 0.5$ 级; 时间,  $\pm 20\%$ 地震复发时间. 目前, 通常采用的是放宽某一个要素的范围, 进而相对准确地预测另外两个. 比如地震中长期概率预报, 根据历史地震和地质构造资料, 圈定地震危险区、评估地震可能达到的最大震级; 在此基础上, 基于对潜在活动断裂地震复发规律的理解, 给出不同震级的地震在不同时间尺度的发生概率<sup>[4,5]</sup>. 此类研究属于基于概率的地震危险性分析(probabilistic seismic ha-

zard analysis, 简称为PSHA), 被广泛应用在地震危险性评估工作中<sup>[6,7]</sup>.

但即使把“三要素”降维到“两要素”, 比如可以通过不同的方法有效地圈定地震危险区<sup>[8]</sup>, 甚至圈定到某一条断裂带, 但针对某一断裂带准确预测地震的震级和时间, 依然十分困难, 因为震级和时间两者存在耦合关系. 震间期越长, 断层上累计的应力越多, 地震可能释放的能量则越高. 然而, 目前对地震成核过程的观测和理解还十分有限<sup>[9,10]</sup>, 不足以准确判断未来地震的发生时间. 此外, 由于断层结构和破裂过程的复杂性, 导致同一断裂带地震破裂可能具有明显的分段性, 即同一断裂带上地震的复发模式并非完全规律的周期性循

引用格式: 杨宏峰, 姚素丽, 陈翔. 非均匀断层上的破裂传播及对震级预测的挑战. 科学通报, 2022, 67

Yang H F, Yao S L, Chen X. Rupture propagation on heterogeneous fault: Challenges for predicting earthquake magnitude (in Chinese). Chin Sci Bull, 2022, 67, doi: [10.1360/TB-2021-1086](https://doi.org/10.1360/TB-2021-1086)

环<sup>[11,12]</sup>. 由于部分断裂带历史地震资料匮乏, 无法准确判断不同段积累能量的差异, 并无法认识这些断裂带上地震发生的规律. 这些因素对准确预测未来大地震的震级和时间带来了挑战.

如果我们考虑继续降低预测要求, 只预测一个要素, 即不考虑时间, 只是针对某一断裂带预测震级, 也依然存在着相当大的挑战. 根据对有效地震预测的期待, 震级的偏差不能超过0.5级<sup>[1]</sup>. 但是, 因为断裂带具有非均匀性(图1), 比如断层几何、断裂带介质结构、断层上的应力分布等, 会不同程度地影响地震破裂的传播和发震震级. 即使在同样的初始条件下, 震级及地表强震动也受到一系列因素的影响, 比如破裂起始的位置——震中<sup>[9,10]</sup>, 断裂带浅部低速带<sup>[13,14]</sup>等. 此外, 中强地震的破裂方向性以及近地表浅部滑移的分布<sup>[15]</sup>, 对于地震灾害评估也至关重要. 对于同等震级的地震, 不同的破裂方向会造成同一位置显著不同的地表震动. 美国加州帕克菲尔德地震试验场观测到的结果显示, 在同一断层地点, 同等震级的地震, 破裂方向甚至可以截然相反<sup>[16]</sup>. 在其他地区, 部分地震造成了较大的浅部滑移和地表破裂, 如2014年云南鲁甸6.4级地震造成的灾害损失远超2014年的云南景谷6.4级地震, 后者则具有典型的浅部滑移亏损<sup>[15]</sup>. 再如2022年青海门源6.9级地震, 造成了超过22 km的地表破裂<sup>[17]</sup>, 致使兰新高铁线路严重受损、列车停运. 尽管不同方法都预估此次门源地震所在的冷龙岭断裂有发生强震的可能<sup>[18-20]</sup>, 并根据滑移亏损估算了未来地震的矩震级为7.2~7.5<sup>[19,20]</sup>, 但实际发震的矩震级为6.7<sup>[17]</sup>, 且伴随着明显的地表破裂, 这在事前震害评估中难以预测. 本文聚焦于断裂带的非均匀性, 回顾相关因素对地震破裂传播和震级的影响, 探讨未来基于震源物理应对地震灾害评估的手段及其效果.

## 1 影响地震破裂传播的因素

### 1.1 应力分布与摩擦属性

地震破裂现象是断层上累积的应力快速释放的过程. 断层上的应力分布对地震的发生和破裂传播过程具有关键性作用. 因此, 断层是否存在应力积累是判断地震危险性的重要依据. 由于地震发生位置一般位于地表以下几千米, 在这一深度下, 断层应力状态基本没有直接测量数据进行约束. 即使如此, 地震观测表明, 断层上的应力分布具有非均匀性. 例如2008年汶川8.0级地震的主破裂区域由几个高滑移块体组成, 其滑移和应力降分布呈现不均匀性<sup>[21,22]</sup>. 在大地震中, 此类滑移不均匀分布的特征能够被广泛观测到, 如1999年土耳其7.5级Izmit地震<sup>[23]</sup>、2010年智利8.8级Maule地震<sup>[24]</sup>、2015年智利8.3级Illapel地震<sup>[25]</sup>和尼泊尔7.8级地震<sup>[26]</sup>、2021年中国7.4级玛多地震<sup>[27]</sup>等. 除同震观测外, 震间期的大地测量观测表明, 许多断层沿走向呈现蠕滑和闭锁相间分布的特点, 体现出断层上应力积累的横向不均匀性, 如美国阿拉斯加俯冲带断层<sup>[28]</sup>和中国西南部的安宁河断层<sup>[29,30]</sup>. 除了沿断层走向的变化, 应力积累在深度上也存在变化. 比如在中美洲尼科亚半岛下方的俯冲带, 闭锁程度由浅到深呈现强-弱-强的变化<sup>[31,32]</sup>.

断层处于蠕滑或闭锁状态, 是否存在应力积累, 其决定条件是断层的摩擦属性. 若介质材料表现出速度强化的特征, 即摩擦阻力随滑动速率增加而增加, 断层则趋向于稳定的慢速蠕滑; 而在速度弱化区, 断层摩擦阻力随速度增加而下降, 使断层运动得以加速、从而发生地震. 一般而言, 岩石的摩擦属性随温度变化, 低温下岩石受力产生脆性变形且表现为速度弱化, 随着温度上升, 岩石开始出现韧性变形且速度强化. 实验室

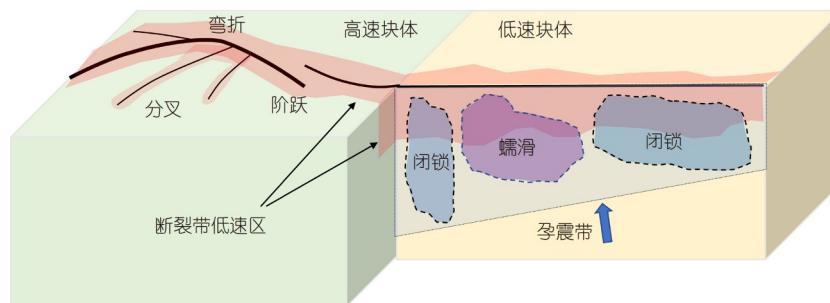


图1 (网络版彩色)断层几何、断裂带介质属性、孕震带结构与应力分布的非均匀性示意图

Figure 1 (Color online) Schematic plot showing the heterogeneities in the fault geometry, the material properties, the structure of seismogenic zones, and the stress condition

测量结果能够证实这一规律。如花岗岩,从速度弱化到强化的转换点温度大约为 $300\sim 350^{\circ}\text{C}$ <sup>[33]</sup>;而玄武岩样品则可以在更高温度范围(约 $600^{\circ}\text{C}$ )保持速度弱化的特征<sup>[34]</sup>。断层浅部,由于岩石结构相对松散,摩擦时易产生膨胀效应导致强化<sup>[35]</sup>。随着深度增加,岩石被压实,此效应减弱。基于以上原因,地壳内断层的孕震区大部分位于 $3\sim 15\text{ km}$ 深度范围。除随深度变化外,断层的摩擦属性还存在横向不均匀性。此类变化大多来自于材料成分差异。若断层泥中含有较多的有机物成分和黏土矿物,如蒙脱石、云母等,在相对低温下仍能呈现速度强化特征的物质,则可能造成在孕震深度的蠕滑现象<sup>[36-38]</sup>。

断层上摩擦性质的非均匀性会影响破裂的传播范围。地震成核只发生在孕震区,即速度弱化区;速度强化区不支持地震成核,且会抑制破裂传播。数值模拟研究表明,孕震带深部的速度强化区能限制地震破裂的深度<sup>[39]</sup>;若速度弱化区和强化区在同一深度相间分布,破裂是否能突破强化区继续传播取决于其具体的摩擦性质以及破裂能量释放大小<sup>[40]</sup>;若断层近地表浅部存在速度强化区,会导致断层滑移速率减小并抑制超剪切破裂的形成。但取决于速度强化区的大小,破裂仍有可能到达地表<sup>[39,41]</sup>。

即使在孕震区内,应力和摩擦性质的不均匀对地震破裂过程也会产生重要的影响。地震是断层克服摩擦阻力快速滑动的过程。当剪切应力超过断层摩擦强度,即最大静摩擦力,断层开始滑动。因此,断层局部应力与其摩擦强度之间的差距决定了破裂传播的尺度。在非均匀应力加载的条件下,地震破裂趋向于发生在高应力加载区并开始传播,然后在低应力区减弱或停止,形成地震分段<sup>[9,10]</sup>。但这种现象并非绝对,如破裂遇到断层上高摩擦强度的障碍体时(高正应力),也可能越过障碍体并激发超剪切破裂<sup>[42]</sup>,这一现象发生与否取决于障碍体的强度以及破裂过程能量的大小。就更小尺度而言,断层非均匀性影响地震波能量频率。非均匀分布增加了破裂过程的复杂性,地面运动高频能量增加。与此同时,应力的不均匀性会抑制连续的超剪切传播和马赫波的形成。在这种情况下,地面高频能量相对均匀应力下的超剪切破裂情景会有所降低<sup>[43]</sup>。

## 1.2 震中位置

由于断层上应力和摩擦强度的分布存在不均匀性,地震成核(震中)的位置也存在不确定性。根据目前对地

震物理过程的认识,在地震发生之前,对于地震到底在哪里成核缺乏有效的判断依据。即使地震发生之后,确定震中位置也常常因为数据的覆盖欠缺以及地下速度结构的不确定性,导致一定程度的误差(几百米至几千米)<sup>[44-46]</sup>。而破裂动力学模拟的结果显示,在应力非均匀分布的断层上,不同的成核位置,即使两个成核地点相互邻近并且所在位置的初始应力相同(图2(a)),最终地震的破裂范围和震级也会存在较大区别<sup>[9]</sup>。例如,在中美洲尼科亚俯冲带内,利用震间闭锁模型计算得到应力分布(图2(a)),选取临近的震中位置开展动力学模拟,结果发现,不同震中位置对应的最终震级相差可能超过2.0(图2(b)-(d))。

除影响震级大小外,地震滑移随深度的分布也受到震中位置的影响。在针对安宁河断裂带的动力学模拟结果中,同样利用震间闭锁得到应力分布(图3(a))。当破裂起始点发生变化时,有的破裂会成为自停止破裂(图3(b)),形成中等强度的地震;有的会导致大地震,但破裂不会到达地表(图3(c));有的则可能会冲破地表,造成严重的近地表位移(图3(d)),震害严重。在后面两种情况中,两者的震级相差0.2,并且成核区都处于高应力区,甚至未能到达地表的破裂起始位置所在的应力更高,这说明浅部滑移分布与震中位置的应力高低并非呈简单的正比关系。这种与震中位置相关的破裂情景,物理机制源于破裂前缘释放能量与断层破裂能的空间分布<sup>[10]</sup>。因为非均匀应力分布状态的存在,导致破裂前缘能量释放率与震中位置密切相关,而破裂前缘的能量释放率会决定破裂的空间展布尺度和滑移大小,也就决定了最终震级。

## 1.3 断裂带介质结构

除了断层面上的特征,断层周围的介质属性对断层上的地震破裂发展也有着重要影响。在近断层的观测尺度上,介质存在较强的非均匀性。由于近断层区域在历史地震中经历了强烈的地面运动,该区域常伴有断层破碎带<sup>[47-50]</sup>,这类破碎带由高度破碎的岩石材料组成,呈现出较低地震波速的地震学特征,因此也被称为近断层低速带。近断层破碎带的跨断层宽度通常在几十米到几千米的量级,其地震波速度相比围岩低约 $20\%\sim 50\%$ <sup>[51-55]</sup>。作为一种常见的近断层非均匀特征,断层破碎带不仅能放大地震波的地表震动<sup>[56,57]</sup>并引入复杂的波场,更能对断层面上的地震破裂过程产生影响。数值模拟的研究表明,断层破碎带的存在能够扩大

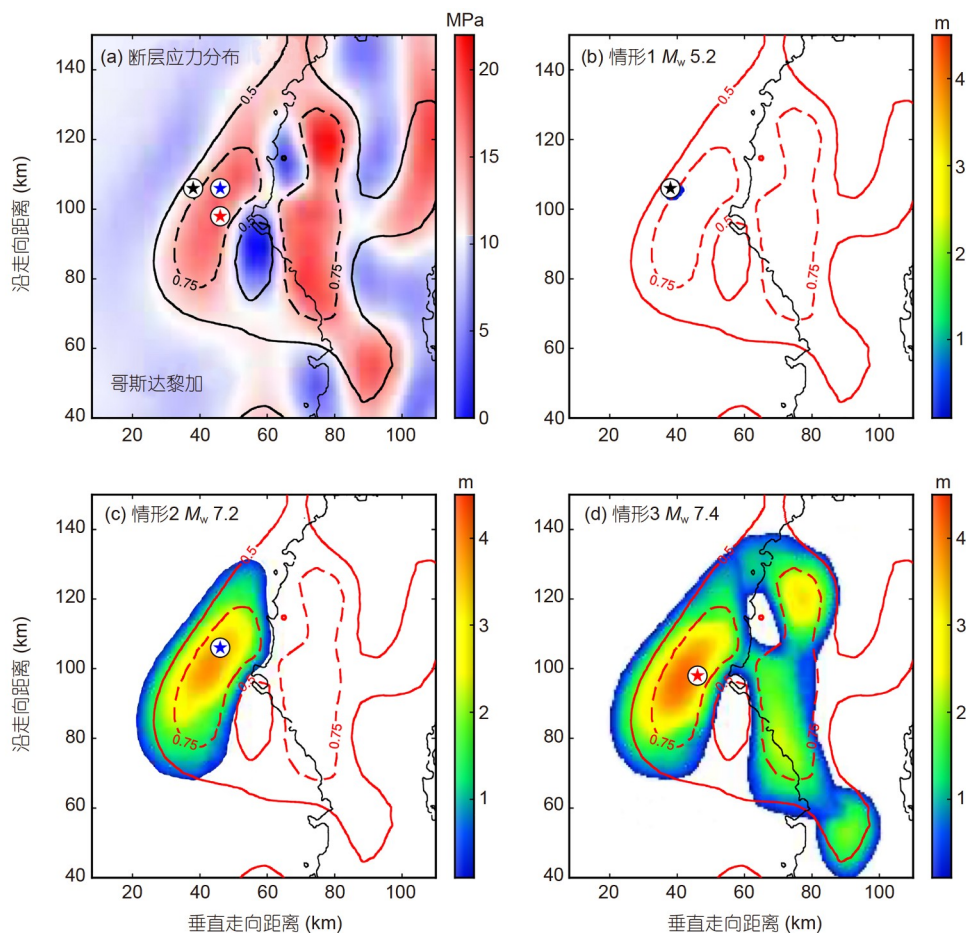


图2 中美洲尼科亚俯冲带上非均匀应力分布(a)以及不同震中位置(不同颜色五角星)所对应的动力学地震模型(b)~(d). (a)中的应力分布由闭锁模型计算得到. (b)~(d)中颜色代表最终滑移分布. 虚线和实线分别圈定了断层上闭锁程度大于75%、60%的区域. 修改自文献[9]

**Figure 2** Heterogeneous stress distribution (a) and dynamic rupture models with different nucleation locations (the pentagrams in different colors) (b)~(d) on the Nicoya megathrust in Central America. The stress condition in (a) is derived from a locking model. The color in (b)~(d) represents the final slip distribution. The dashed and solid contours indicate the areas with locking degree over 75% and 60%, respectively. Modified from Ref. [9]

地震的破裂延伸范围并影响地震震级的最终大小<sup>[13]</sup>; 主要机制是碎带界面引入的反射波与首波等复杂的地震波场调节了断层上破裂的传播速度以及滑移模式<sup>[58,59]</sup>. 断层低速带的存在也会影响由地面观测估算断层面的摩擦参数结果, 造成高估的情况<sup>[60]</sup>.

此外, 断层的周边介质速度结构还可能存在跨断层两侧的不对称性, 即断层两侧存在物质差异, 又称为双材料结构<sup>[61,62]</sup>. 断层两侧的物质差异取决于断层的形成过程与环境, 差异程度可以由地震波速度成像揭示, 在多个断层带均有发现. 如玉树地震的发震断层面上, 断层带首波研究观测到5%~8%的波速差异<sup>[63]</sup>; 北安纳托利亚断层两侧约有6%的纵波速度差异<sup>[64]</sup>; 圣安德烈斯断层两侧的介质地震波速度差在5%~30%之

间<sup>[62]</sup>. 这种断层的双材料结构可影响地震破裂发展的方向性, 从而影响断层周围的地表震动与灾害分布. 破裂动力学模拟研究显示, 当断层两侧介质存在速度差异时, 地震破裂将存在一个优先破裂的方向, 与较慢波速一侧介质的运动方向一致<sup>[61]</sup>. 考虑双材料结构的影响并估计优先破裂方向, 对于区域地震灾害评估, 尤其是在人口聚集区具有积极的意义.

#### 1.4 孕震带尺度

断层上孕震带区域的几何特征可以影响地震破裂的发展和传播. 作为地震破裂发生的区域, 孕震带的空间范围是有界的. 由于受到地壳内温压条件的影响, 地震破裂只能发生在一定的深度范围内<sup>[65,66]</sup>, 从而限制

孕震带在沿断层倾向的宽度。作为孕震带的一项基本几何特征,孕震带的有限宽度影响着地震破裂的发展。观测数据表明,倾滑地震的破裂长度随宽度的增加而增加,两者之间的比值一般不超过8(图4(a));但走滑地震则不同,当破裂达到整个孕震带宽度(孕震带饱和现象)前后,地震破裂的震源参数存在着不同的尺度关系<sup>[67~70]</sup>,破裂的长度/宽度比具有很大的变化(图4(b))。

部分走滑地震( $M_w > 7$ )的破裂长度远超其破裂宽度,其比值高达40(图4(b))。观测数据表明,孕震带的宽度对破裂的发展及最终地震的震级存在着控制作用,而破裂动力学数值模拟研究也揭示了其内在的机理<sup>[71]</sup>。若走滑断层孕震带宽度有限( $< 10$  km),破裂会成为自停止模式(self-arresting),震级有限;随着孕震带宽度的增大,同等初始条件下地震破裂的模式会从自停止破裂

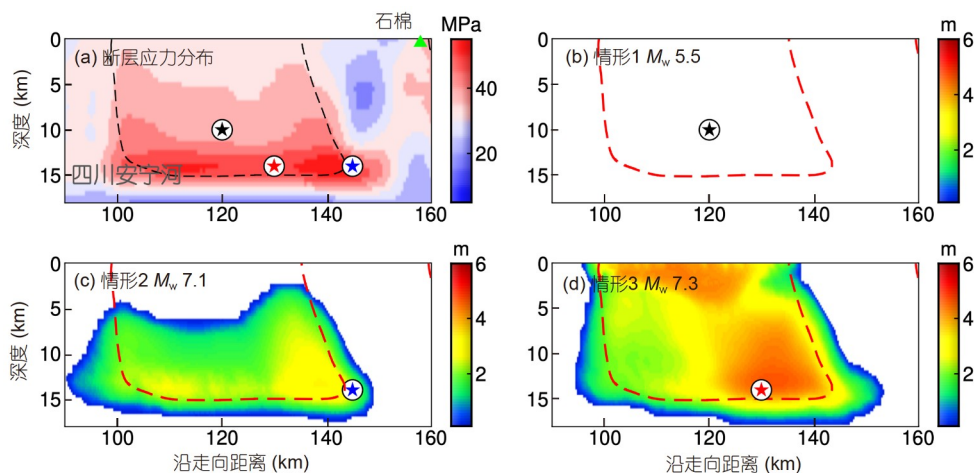


图3 安宁河断层应力分布(a)以及不同震中位置(不同颜色的五角星)对应的破裂情景(b)~(d)。(a)中应力分布是基于闭锁模型计算得到。(b)~(d)中颜色代表最终滑移分布,五角星代表模型震中位置。(a)~(d)中虚线代表闭锁程度大于75%的区域。走向朝北,参考点为(102.0°E, 27.8°N)。修改自文献<sup>[10]</sup>

Figure 3 The stress condition and the rupture scenarios with different hypocenters (pentagrams in different colors) (b)~(d) on the Anninghe fault. The stress condition in (a) is derived from a locking model. The color in (b)~(d) represents the final slip distribution. The dashed lines indicate the area with locking degree over 75%. The strike is toward north. The reference point is (102.0°E, 27.8°N). Modified from Ref. <sup>[10]</sup>

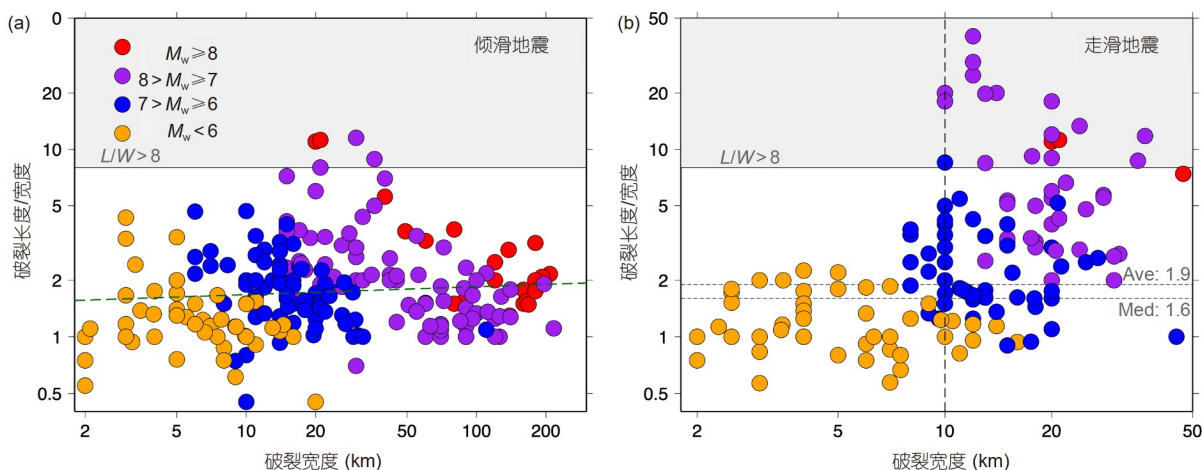


图4 倾滑(a)与走滑地震(b)的破裂长度/宽度比值( $L/W$ )与破裂宽度的关系。如(a)中虚线所示,倾滑地震两者之间的线性拟合斜率为0.04。如(b)中虚线所示,震级小于7的走滑地震破裂长宽比的平均值与中位数分别为1.9和1.6

Figure 4 The ratio of the rupture length to the width ( $L/W$ ) versus the rupture width in dip-slip earthquakes (a) and strike-slip earthquakes (b). The dashed line in (a) represents the linear regression of the dataset of dip-slip earthquakes with a slope of 0.04. The dashed lines in (b) stand for the mean (1.9) and the median (1.6) values for the ratio of rupture length to width among strike-slip events with magnitude less than 7

向逃逸(breakaway)破裂转化,造成更大的地震破裂规模和最终地震震级.同时,孕震带宽度也能影响近断层地表运动,并影响从地表估算摩擦参数的视趋势<sup>[60]</sup>.

在一些较长的断层上,孕震带的几何特征还存在沿走向的变化,并影响断层上的破裂发展.例如孕震断层在走向方向上的弯曲<sup>[72,73]</sup>、断层的分支<sup>[74,75]</sup>、断层的阶跃<sup>[76-79]</sup>等.除了这些多断层的特征,在单一断层上,孕震带的宽度也可能存在着走向上的变化.数值模拟的实验结果表明,孕震带宽度沿走向的变化可以影响地震破裂的方向性.在一个孕震带宽度沿走向增加的断层上,相比于较窄的一侧,大地震破裂更倾向于从较宽的一侧开始<sup>[80]</sup>.地震的方向性会在很大程度上影响地震周边的灾害情况<sup>[56,81]</sup>.因此,认识孕震带宽度及其空间上的变化对地震破裂发展的影响对于地震灾害的灾前预估有着重要意义.

上述讨论均基于断层无横向应力变化,仅存在孕震区宽度变化的情况.由于断层上的应力与摩擦性质存在不均匀性,断层的孕震能力沿走向可能存在明显的变化,导致当地震从不同位置开始破裂时,其所能用于地震传播的能量存在区别,即前文讨论的震级与震中的依赖关系. Yang等人<sup>[9]</sup>引入“有效孕震带”的概念,即在非均匀应力下,地震的“有效孕震带”取决于地震初始位置周围的应力水平.因为破裂得以传播的物理

条件是应力水平要超过摩擦强度(图5(c)),能否克服两者之间的差距(strength excess, 强度盈余)便成为破裂前缘是否延续或者终止的先决条件.若断层上的强度与应力分布都比较均匀,则两者之间的差距也基本一致,破裂从成核区域开始后,破裂前缘释放的能量可以克服强度盈余,利于传播到更远处,形成大地震(图5(a));反之,破裂成核后,破裂前缘迅速到达强度很高或应力很低的区域,其能量不够克服强度盈余,则破裂会停止(图5(b)).这也是前面所述“震中-震级”之间相互依赖而导致“震级测不准”的原因所在.

## 2 非均匀断层的地震危险性评估

### 2.1 非均匀断层的地震分段与震级预测

地震震级是地震灾害评估中的重要指标之一,通常利用震间闭锁分布、地震空区、历史地震等界定.比如,在中美洲尼科亚半岛下方存在一个闭锁块体<sup>[31,32]</sup>,由其大小及滑移亏损速率估计,该区域特征地震最大震级约为7.8.对于具有多个闭锁区域的断层系统,该区发生地震的震级大小取决于块体大小以及是否发生级联破裂,这些区域震级分布复杂且非连续.如中国西南部的鲜水河-安宁河-则木河走滑断层系统,历史地震记录显示,该断层系统存在复杂的分段性<sup>[11]</sup>.在

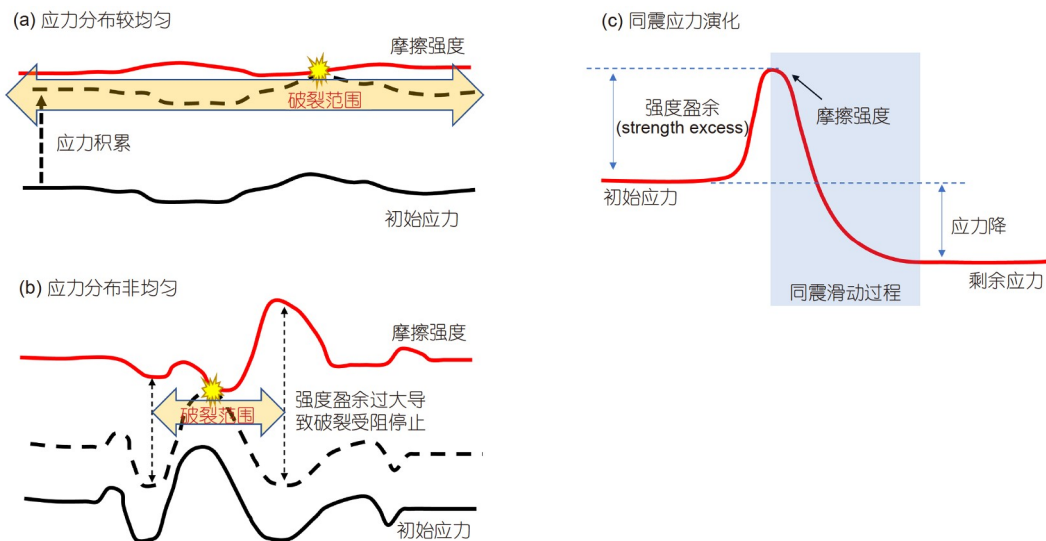


图 5 断层应力与摩擦强度不均匀性对地震破裂范围影响的示意图(a, b)和同震过程中断层应力演化示意图(c). (a)和(b)中的红线代表断层面上的摩擦强度,黑色实线代表初始应力分布,黑色虚线表示应力水平积累到发生地震的程度,破裂由震中(黄色爆炸星星)开始向断层两侧传播  
Figure 5 Schematic plots showing the influence of heterogeneous fault stress and frictional strength on the rupture propagation (a, b) and stress evolution on faults during an earthquake (c). Red and black solid lines in (a) and (b) represent frictional strength and stress on the fault while black dashed line shows the accumulated stress level at which an earthquake occurs. The rupture initiates at the yellow explosion symbol and propagates along the fault bilaterally

安宁河断层中段和南段均出现了分段, 南段内部存在两个闭锁块体<sup>[29]</sup>, 该区历史地震中单独破裂和级联破裂均有发生, 故震级估算为 $6^{3/4}$ 和 $7^{1/2}$ <sup>[11]</sup>; 又如北美卡斯卡迪亚俯冲带断层, 历史上出现过横贯整个俯冲带的超强地震(9级), 也有相当数量的地震仅破裂了俯冲带南段<sup>[12]</sup>. 目前, 断层系统的破裂分段行为没有统一的规律性, 仅根据历史地震序列无法直接判断下次大地震震级.

针对由断层非均匀性导致的“震中-震级测不准关系”, 对目标断层开展地震动力学模拟是一个可行的手段. 事实上, 地震动力学数值模拟已经被广泛应用于地震情景构建, 包括现代及历史地震<sup>[82]</sup>. 若与目标断层的地质背景、滑移速率、能量积累等结合, 可应用于非均匀断层上的未来地震震级预测. 以中美洲俯冲带尼科亚半岛为例(图6(a)), 该地俯冲速率达 $\sim 82$  mm/a, 地震频繁. 基于震间闭锁模型开展的动力学模拟结果显示, 在震中位于中高闭锁程度区域的模型中, 破裂可以

发展成为7级以上甚至超过7.6级的大地震; 但从其他震中开始的破裂都是低于6级的中等地震, 形成了一个6~7级之间的震级空区(图6(b), (c)). 而在该区域的地震目录中, 俯冲界面上的地震震级也大多低于5.5级, 包括2012年7.6级地震之后的余震活跃时期(图6(d)). 该地区的动力学模拟结果与观测结果高度吻合<sup>[83]</sup>, 表明了利用地震动力学模拟来预测震级的可行性.

地震破裂受断层上应力水平、摩擦性质, 以及断层结构共同控制. 因此, 开展可靠的动力学模拟, 需要对上述因素进行合理约束. 我们可以通过地震学方法研究断层结构. 目前, 基于密集台阵的断裂带成像、地震精定位等手段都可用于刻画断层结构<sup>[54,84,85]</sup>, 一系列基于密集台阵的新方法得到了发展<sup>[57,86,87]</sup>. 约束断层在孕震深度的应力分布缺乏直接的测量数据. 最有效的方法是利用现代大地测量手段, 反演震间期断层上的闭锁程度分布, 进而计算断层上的应力分布, 圈定断层的高应力块体<sup>[9,10,83]</sup>. 由于断层摩擦属性很难进行直接

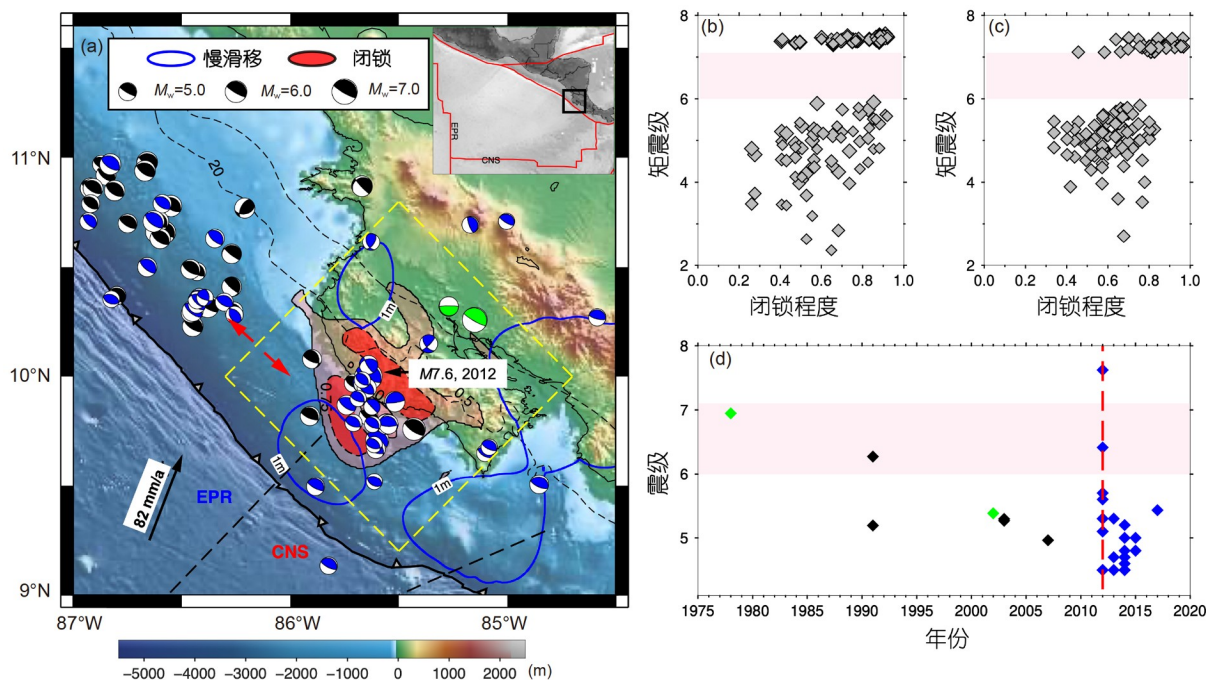


图6 中美洲俯冲带尼科亚半岛地区闭锁(a)及地震震级分布(b)~(d). (a) 尼科亚区域震间闭锁(红色区域)分布、慢速滑移区域(蓝色实线内)、及逆冲地震的震源机制解. EPR: 东太平洋海隆; CNS: 科克斯-纳兹卡扩展脊. (b), (c) 由两个震间闭锁模型预测得到闭锁程度与震级的关系. (d) 尼科亚半岛地区((a)中黄色虚线部分)俯冲界面地震的震级随时间的分布. 黑色: 2012年7.6级地震之前; 蓝色: 2012年7.6级主震及余震; 绿色: 闭锁范围之外的地震. (b)~(d)中的粉色区域表示震级缺失范围. 修改自文献<sup>[9]</sup>

Figure 6 Locking and earthquake magnitudes in Nicoya region. (a) Map for the Nicoya region with the distribution of the interseismic locking (red area), slow slip (blue contours), and focal mechanisms of thrust earthquakes. EPR: Eastern Pacific Rise, CNS: Cocos-Nazca Spreading Center. (b) and (c) represent the predicted magnitudes of future earthquakes versus the locking degree from two locking models. (d) The temporal evolution of seismicity on Nicoya megathrust (the region inside the dashed yellow rectangle in (a)). Earthquakes before and after the 2012  $M_w$  7.6 earthquake are plotted in black and blue, respectively. Earthquakes outside the locked zone are marked in green. The magnitude gap is marked in pink in (b)~(d). Modified after Ref. <sup>[9]</sup>



约束,主要参考实验室摩擦实验结果<sup>[88]</sup>,或利用近场观测结合动力学参数反演的方法约束不同地质条件下的同震摩擦属性<sup>[89,90]</sup>。结合以上非均匀断层性质进行动力学模拟,可观察地震是否能突破块体间的低应力区,并得到未来可能的地震情形<sup>[9,10,91]</sup>。

除动力学模拟外,Noda等人<sup>[92]</sup>从能量平衡的角度,计算断层已经积累的弹性能和地震所消耗的能量(摩擦热和断裂能的总和),判断块体是否能破裂甚至发生穿越不同块体的级联破裂。其原理表述如下:累积弹性能远大于破裂传播所消耗的能量,则破裂可以持续传播,最终产生大地震。但计算断裂能和摩擦生热都基于关键同震摩擦参数的数值。如前所述,目前估算发震断层的摩擦属性尚存挑战<sup>[90,93]</sup>,参数的估计也存在相当的不确定性。据此估算未来地震的震级也存在相当的不确定性。

## 2.2 地面运动多变性与灾害评估

除了地震的最终震级,地面运动强度预测是地震灾害评估中非常重要的一环。目前,绝大部分灾害评估采用经验预测公式(empirical ground motion prediction equations, GMPEs)对地震可能产生的地面运动强度进行预测<sup>[94,95]</sup>。在GMPEs中,地震引起的地面运动强度主要受到地震震级、震中距、传播介质属性(尤其为近地表速度结构,比如地下30 m的剪切波速度结构 $V_s(30)$ )控制。然而,对于复发周期长的大地震,此类经验预测公式通常缺乏近场数据。而近场地面运动受到地震破裂过程的影响较为剧烈,其破裂过程,包括破裂方向<sup>[96]</sup>以及地表破裂分布<sup>[97]</sup>等,对近场地面运动灾害分布起到至关重要的作用,这对于经验公式在大地震预测中的应用提出了挑战。

未来,基于非均匀断层的动力学破裂模型可用于预测大地震地面运动<sup>[98,99]</sup>。上文提到,地震的破裂方向性可能受到断层物质属性及孕震带结构的影响,需要结合动力学模型进行判断。即使断层性质已知,地震从不同位置起破依然会引起不同的方向性和地面响应。如在俯冲带,当地震从深部成核向海沟处传播时,容易引起较大的浅部滑移和海底隆升,增加海啸风险<sup>[9]</sup>。走滑断层在非均匀应力条件下,不同的起破点位置可能会造成不同的浅部滑移分布和地表破裂分布<sup>[10]</sup>,导致断层周围地面响应剧烈变化。由于未来地震的震中未知,需要测试不同的震中位置以理解破裂过程的多变性。断层不均匀性和动力学模拟得到未来大地震的可

能破裂情形及地面响应,与传统的GMPEs相结合,可以更加全面地评估未来地震所造成的灾害分布。

## 3 总结与展望

本文简要回顾了影响地震破裂传播的因素,并指出目前针对地震震级预测的一系列可行性手段及面临的挑战。导致目前震级、破裂方向性、近地表滑移分布等要素不确定性的核心问题是,发震断层上的介质与几何结构、应力分布具有不同尺度的非均匀性。相应地,如何刻画断层结构的非均匀性,以及如何考虑断层的各种非均匀性来判定和理解地震破裂尺度与震级,是未来需要关注的问题。

与介质结构相比,断层几何和应力分布对破裂的影响更大。刻画断层几何形态通常结合地质构造填图、地震精定位、地震反射方法和地震成像等手段。但对于没有良好观测覆盖或者现今地震稀少的区域,对断裂深部形态的约束以及盲(隐伏)断层的刻画存在较大困难。针对这些区域,可以采取综合地球物理探测方法,约束断层几何形态。

尽管断层的应力分布对地震破裂传播过程非常关键,然而现今手段对地壳深部的应力测量依然困难重重,目前更多的是采用间接手段。尽管通过大地测量、历史地震震源机制等可以推测应力场方向,但是发震断层上的绝对应力水平则很难约束。此外,流体分布与孔隙流体压力的大小,也直接影响断层摩擦强度的高低。热流测量以及同震过程等观测和模拟手段表明,断层发震深度的孔隙流体压力应该高于静水压、接近静岩压<sup>[90,100,101]</sup>,尤其是板块边界的断层。但是,许多陆内断层的构造不一,孔隙压力是否遵循静水压或近静岩压的变化规律则需要更多观测验证。通过研究小地震震群活动规律与某些已知应力扰动的关系,如远震动态触发<sup>[102-104]</sup>、潮汐<sup>[105]</sup>等,可以帮助量化目标断层的当前强度盈余。但是能否为中强地震破裂尺度范围提供约束,取决于被触发的小地震震群空间分布,目前依然需要深入研究。

相较之下,确定断裂带介质结构得益于地震台阵观测,特别是短周期密集台阵的快速增加。针对断裂带进行多尺度地震成像的工作已在多地展开,包括中国四川安宁河断裂带<sup>[84]</sup>、云南宾川程海断裂带<sup>[50,106]</sup>等。近期更有新的观测手段比如光纤技术被应用于刻画地下精细结构<sup>[107]</sup>,未来有望在断裂带精细结构成像获得进一步突破。针对断裂带进行地震层析成像,并与历史

地震的破裂尺度进行关联的研究很多。但是各地的构造不同,地震破裂尺度以及发生位置与层析成像的结果到底是何种关系,尚需进一步研究与讨论。值得注意的是,部分成像结果发现,一些中强地震发生在地壳速度结构变化的位置,比如高速-低速转换带。这本在意料之中,因为此处是断裂带所在的位置,而断裂带两侧的介质速度结构本就可能存在差异。是否能利用地壳速度空间梯度来指示未来强震位置,还需进一步探讨。

也有部分研究指出,断裂带沿走向的速度结构呈

现非均匀性,并在个别区域与地震破裂的尺度吻合。但目前应用的实例有限,并且成像的分辨率通常在数千米至十千米量级,远远大于断裂带的宽度。若成像的分辨率可提高至近断层尺度(百米),则可以结合实验室的流变实验结果<sup>[108]</sup>,将地震成像的速度结构转为断层流变性质<sup>[109]</sup>,进而约束断层面上的凹凸体分布。在未来地震成像分辨率不断提高的趋势下,地震成像结果有望为约束断层流变结构的非均匀性提供新的视角,为预测未来地震震级提供理论基础。

**致谢** 感谢两位匿名评审的中肯意见,帮助作者大幅提升了本文质量。感谢中国地震台网中心徐沁提供的文字校对。

## 参考文献

- Chen Y T. Earthquake prediction: Retrospect and prospect (in Chinese). *Sci China Ser D Earth Sci*, 2009, 39: 1633–1658 [陈运泰. 地震预测: 回顾与展望. *中国科学: 地球科学*, 2009, 39: 1633–1658]
- Wu Z L, Wang L, Li L, et al. China seismic experimental site (CSES): Earthquake forecast and system design (in Chinese). *Rev Geophys Planet Phys*, 2021, 52: 679–683 [吴忠良, 王龙, 李丽, 等. 中国地震科学实验场: 地震预测与系统设计. *地球与行星物理理论评*, 2021, 52: 679–683]
- Shi Y L, Sun Y Q, Luo G, et al. Roadmap for earthquake numerical forecasting in China—Reflection on the tenth anniversary of Wenchuan earthquake (in Chinese). *Chin Sci Bull*, 2018, 63: 1865–1881 [石耀霖, 孙云强, 罗纲, 等. 关于我国地震数值预报路线图的设想——汶川地震十周年反思. *科学通报*, 2018, 63: 1865–1881]
- Xie F R, Zhang S M, Zhang Y Q, et al. Large earthquake recurrence intervals along active faults in mainland of China (in Chinese). *Technol Earthq Disaster Prevent*, 2013, 8: 1–10 [谢富仁, 张世民, 张永庆, 等. 中国大陆活动断裂大震地震复发间隔. *震灾防御技术*, 2013, 8: 1–10]
- Pan H, Gao M T, Xie F R. The earthquake activity model and seismicity parameters in the new seismic hazard map of China (in Chinese). *Technol Earthq Disaster Prevent*, 2013, 8: 11–23 [潘华, 高孟潭, 谢富仁. 新版地震区划图地震活动性模型与参数确定. *震灾防御技术*, 2013, 8: 11–23]
- Cornell C A. Engineering seismic risk analysis. *Bull Seismol Soc Am*, 1968, 58: 1583–1606
- Bommer J J, Akkar S. Consistent source-to-site distance metrics in ground-motion prediction equations and seismic source models for PSHA. *Earthq Spectra*, 2012, 28: 1–15
- Xu X W, Wu X Y, Yu G H, et al. Seismo-geological signatures for identifying  $M$  7.0 earthquake risk areas and their preliminary application in mainland of China (in Chinese). *Seismol Geol*, 2017, 39: 219–275 [徐锡伟, 吴熙彦, 于贵华, 等. 中国大陆高震级地震危险区判定的地震地质学标志及其应用. *地震地质*, 2017, 39: 219–275]
- Yang H, Yao S, He B, et al. Earthquake rupture dependence on hypocentral location along the Nicoya Peninsula subduction megathrust. *Earth Planet Sci Lett*, 2019, 520: 10–17
- Yao S, Yang H. Hypocentral dependent shallow slip distribution and rupture extents along a strike-slip fault. *Earth Planet Sci Lett*, 2022, 578: 117296
- Wen X, Ma S, Xu X, et al. Historical pattern and behavior of earthquake ruptures along the eastern boundary of the Sichuan-Yunnan faulted-block, southwestern China. *Phys Earth Planet Inter*, 2008, 168: 16–36
- Goldfinger C, Nelson C H, Morey A E, et al. Turbidite Event History—Methods and Implications for Holocene Paleoseismicity of the Cascadia Subduction Zone. US Geological Survey Professional Paper 1661-F, 2012. 170
- Weng H, Yang H, Zhang Z, et al. Earthquake rupture extents and coseismic slips promoted by damaged fault zones. *J Geophys Res Solid Earth*, 2016, 121: 4446–4457
- Thakur P, Huang Y, Kaneko Y. Effects of low-velocity fault damage zones on long-term earthquake behaviors on mature strike-slip faults. *J Geophys Res Solid Earth*, 2020, 125: e2020JB019587
- Yang H, Yao S. Shallow destructive earthquakes. *Earthq Sci*, 2021, 34: 15–23
- Fletcher J B, Spudich P. Rupture characteristics of the three  $M \sim 4.7$  (1992–1994) Parkfield earthquakes. *J Geophys Res*, 1998, 103: 835–854
- Yang H, Wang D, Guo R, et al. Rapid report of the 8 January 2022 Menyuan  $M_s$  6.9 earthquake, Qinghai, China. *Earthq Res Adv*, 2022, 2: 100113
- Zhou L, Ji L Y, Li Z J, et al. Study on current deformation process and seismicity of Lenglongling area based on small earthquakes and GPS data (in Chinese). *J Seismol Res*, 2022, 45: 1–7 [周琳, 季灵运, 李长军, 等. 利用小震和GPS资料分析冷龙岭地区现今变形过程与地震活动. *地震*

- 研究, 2022, 45: 1–7]
- 19 Guo P, Han Z J, Jiang W L, et al. Holocene left-lateral slip rate of the Lenglongling fault, northeastern margin of the Tibetan Plateau (in Chinese). *Seismol Geol*, 2017, 39: 323–341 [郭鹏, 韩竹军, 姜文亮, 等. 青藏高原东北缘冷龙岭断裂全新世左旋滑动速率. *地震地质*, 2017, 39: 323–341]
  - 20 Shi F Q, Shao Z G, Zhan W, et al. Numerical modeling of the shear modulus and stress state of active faults in the northeastern margin of the Tibetan Plateau (in Chinese). *Chin J Geophys*, 2018, 61: 3651–3663 [石富强, 邵志刚, 占伟, 等. 青藏高原东北缘活动断裂剪切模量及应力状态数值模拟. *地球物理学报*, 2018, 61, 9: 3651–3663]
  - 21 Xu C, Liu Y, Wen Y, et al. Coseismic slip distribution of the 2008  $M_w$  7.9 Wenchuan earthquake from joint inversion of GPS and InSAR data. *Bull Seismol Soc Am*, 2010, 100: 2736–2749
  - 22 Tong X, Sandwell D T, Fialko Y. Coseismic slip model of the 2008 Wenchuan earthquake derived from joint inversion of interferometric synthetic aperture radar, GPS, and field data. *J Geophys Res*, 2010, 115: B04314
  - 23 Reilinger R E, Ergintav S, Burgmann R, et al. Coseismic and postseismic fault slip for the 17 August 1999,  $M=7.5$ , Izmit, Turkey earthquake. *Science*, 2000, 289: 1519–1524
  - 24 Lin Y N, Sladen A, Ortega-Culaciati F, et al. Coseismic and postseismic slip associated with the 2010 Maule Earthquake, Chile: Characterizing the Arauco Peninsula barrier effect. *J Geophys Res Solid Earth*, 2013, 118: 3142–3159
  - 25 Yin J, Yang H, Yao H, et al. Coseismic radiation and stress drop during the 2015  $M_w$  8.3 Illapel, Chile megathrust earthquake. *Geophys Res Lett*, 2015, 43: 2015GL06738
  - 26 Yin J, Yao H, Yang H, et al. Frequency-dependent rupture process, stress change, and seismogenic mechanism of the 25 April 2015 Nepal Gorkha  $M_w$  7.8 earthquake. *Sci China Earth Sci*, 2017, 60: 796–808
  - 27 Guo R, Yang H, Li Y, et al. Complex slip distribution of the 2021  $M_w$  7.4 Maduo, China, earthquake: An event occurring on a slowly slipping fault. *Seismol Res Lett*, 2022, 93: 653–665
  - 28 Fournier T J, Freymueller J T. Transition from locked to creeping subduction in the Shumagin region, Alaska. *Geophys Res Lett*, 2007, 34: L06303
  - 29 Jiang G, Xu X, Chen G, et al. Geodetic imaging of potential seismogenic asperities on the Xianshuihe-Anninghe-Zemuhe fault system, Southwest China, with a new 3-D viscoelastic interseismic coupling model. *J Geophys Res Solid Earth*, 2015, 120: 1855–1873
  - 30 Li Y, Nocquet J M, Shan X, et al. Heterogeneous interseismic coupling along the Xianshuihe-Xiaojiang fault system, eastern Tibet. *J Geophys Res*, 2021, 126: e2020JB021187
  - 31 Feng L, Zhou T. Water vapor transport for summer precipitation over the Tibetan Plateau: Multidata set analysis. *J Geophys Res*, 2012, 117: B06407
  - 32 Xue L, Schwartz S, Liu Z, et al. Interseismic megathrust coupling beneath the Nicoya Peninsula, Costa Rica, from the joint inversion of InSAR and GPS data. *J Geophys Res Solid Earth*, 2015, 120: 3707–3722
  - 33 Scholz C H. The brittle-plastic transition and the depth of seismic faulting. *Geol Rundsch*, 1988, 77: 319–328
  - 34 Zhang L, He C, Liu Y, et al. Frictional properties of the South China Sea oceanic basalt and implications for strength of the Manila subduction seismogenic zone. *Mar Geol*, 2017, 394: 16–29
  - 35 Marone C, Raleigh C B, Scholz C H. Frictional behavior and constitutive modeling of simulated fault gouge. *J Geophys Res*, 1990, 95: 7007–7025
  - 36 Lockner D A, Morrow C, Moore D, et al. Low strength of deep San Andreas fault gouge from SAFOD core. *Nature*, 2011, 472: 82–85
  - 37 Kohli A H, Zoback M D. Frictional properties of shale reservoir rocks. *J Geophys Res Solid Earth*, 2013, 118: 5109–5125
  - 38 Carpenter B M, Marone C, Saffer D M. Weakness of the San Andreas fault revealed by samples from the active fault zone. *Nat Geosci*, 2011, 4: 251–254
  - 39 Kaneko Y, Lapusta N, Ampuero J. Spectral element modeling of spontaneous earthquake rupture on rate and state faults: Effect of velocity-strengthening friction at shallow depths. *J Geophys Res*, 2008, 113: B09317
  - 40 Kaneko Y, Avouac J P, Lapusta N. Towards inferring earthquake patterns from geodetic observations of interseismic coupling. *Nat Geosci*, 2010, 3: 363–369
  - 41 Yang H, Liu Y, Lin J. Effects of subducted seamounts on megathrust earthquake nucleation and rupture propagation. *Geophys Res Lett*, 2012, 39: L24302
  - 42 Weng H, Huang J, Yang H. Barrier-induced supershear ruptures on a slip-weakening fault. *Geophys Res Lett*, 2015, 42: 4824–4832
  - 43 Bizzarri A, Dunham E, Spudich P. Coherence of Mach fronts during heterogeneous supershear earthquake rupture propagation: Simulations and comparison with observations. *J Geophys Res*, 2010, 115: B08301
  - 44 Zhang Y, An Y, Long F, et al. Short-term foreshock and aftershock patterns of the 2021  $M_s$  6.4 Yangbi earthquake sequence. *Seismol Res Lett*, 2022, 93: 21–32

- 45 Zhou P, Ellsworth W, Yang H, et al. Machine learning facilitated earthquake detections near the Weiyuan shale gas blocks, Sichuan, China. *Earth Planet Phys*, 2021, 5: 503–521
- 46 Wong W C J, Zi J P, Yang H F, et al. Spatial-temporal evolution of injection induced earthquakes in Weiyuan area by machine-learning phase picker and waveform cross-correlation. *Earth Planet Phys*, 2021, 5: 485–500
- 47 Ben-Zion Y, Sammis C G. Characterization of fault zones. *Pure Appl Geophys*, 2003, 3-4: 677–715
- 48 Kim Y S, Peacock D C P, Sanderson D J. Fault damage zones. *J Struct Geol*, 2004, 26: 503–517
- 49 Wu C, Peng Z, Ben-Zion Y. Non-linearity and temporal changes of fault zone site response associated with strong ground motion. *Geophys J Int*, 2009, 176: 265–278
- 50 Yang H, Duan Y, Song J, et al. Illuminating high-resolution crustal fault zones and temporal changes using multi-scale dense arrays and airgun sources. *Earthq Res Adv*, 2021, 1: 2772–4670
- 51 Yang H, Zhu L. Shallow low-velocity zone of the San Jacinto fault from local earthquake waveform modelling. *Geophys J Int*, 2010, 183: 421–432
- 52 Yang H, Zhu L, Cochran E S. Seismic structures of the Calico fault zone inferred from local earthquake travel time modelling. *Geophys J Int*, 2011, 186: 760–770
- 53 Yang H, Li Z, Peng Z, et al. Low-velocity zones along the San Jacinto fault, southern California, from body waves recorded in dense linear arrays. *J Geophys Res Solid Earth*, 2014, 119: 8976–8990
- 54 Yang H, Duan Y, Song J, et al. Fine structure of the Chenghai fault zone, Yunnan, China, constrained from teleseismic travel time and ambient noise tomography. *J Geophys Res*, 2020, 125: e2020JB019565
- 55 Yang H. Recent advances in imaging crustal fault zones: A review. *Earthq Sci*, 2015, 28: 151–162
- 56 Kurzon I, Vernon F L, Ben-Zion Y, et al. Ground motion prediction equations in the San Jacinto fault zone: Significant effects of rupture directivity and fault zone amplification. *Pure Appl Geophys*, 2014, 171: 3045–3081
- 57 Song J, Yang H. Seismic site response inferred from records at a dense linear array across the Chenghai fault zone, Binchuan, Yunnan. *J Geophys Res-Solid Earth*, 2022, 127: e22710
- 58 Huang C S, de La Beaujardiere O, Roddy P A, et al. Evolution of equatorial ionospheric plasma bubbles and formation of broad plasma depletions measured by the C/NOFS satellite during deep solar minimum. *J Geophys Res*, 2011, 116: A03309
- 59 Huang Y, Ampuero J P, Helmberger D V. Earthquake ruptures modulated by waves in damaged fault zones. *J Geophys Res Solid Earth*, 2014, 119: 3133–3154
- 60 Chen X, Yang H. Effects of seismogenic width and low-velocity zones on estimating slip-weakening distance from near-fault ground deformation. *Geophys J Int*, 2020, 223: 1497–1510
- 61 Ben-Zion Y, Shi Z. Dynamic rupture on a material interface with spontaneous generation of plastic strain in the bulk. *Earth Planet Sci Lett*, 2015, 236: 486–496
- 62 Shi Z, Ben-Zion Y. Dynamic rupture on a bimaterial interface governed by slip-weakening friction. *Geophys J Int*, 2006, 165: 469–484
- 63 Yang W, Peng Z, Wang B, et al. Velocity contrast along the rupture zone of the 2010  $M_w$  6.9 Yushu, China, earthquake from fault zone head waves. *Earth Planet Sci Lett*, 2015, 416: 91–97
- 64 Bulut F, Ben-Zion Y, Bohnhoff M. Evidence for a bimaterial interface along the Mudurnu segment of the North Anatolian fault zone from polarization analysis of P waves. *Earth Planet Sci Lett*, 2012, 327-328: 17–22
- 65 Scholz C H. Earthquakes and friction laws. *Nature*, 1998, 391: 37–42
- 66 Marone C. Laboratory-derived friction laws and their application to seismic faulting. *Annu Rev Earth Planet Sci*, 1998, 26: 643–696
- 67 Romanowicz B. Strike-slip earthquakes on quasi-vertical transcurrent faults: Inferences for general scaling relations. *Geophys Res Lett*, 1992, 19: 481–484
- 68 Wells D L, Coppersmith K J. New empirical relationships among magnitude, rupture length, rupture width, rupture area, and surface displacement. *Bull Seismol Soc Am*, 1994, 4: 974–1002
- 69 Romanowicz B, Ruff L J. On moment-length scaling of large strike slip earthquakes and the strength of faults. *Geophys Res Lett*, 2002, 29: 45
- 70 Leonard M. Earthquake fault scaling: Self-consistent relating of rupture length, width, average displacement, and moment release. *Bull Seismol Soc Am*, 2010, 100: 1971–1988
- 71 Weng H, Yang H. Seismogenic width controls aspect ratios of earthquake ruptures. *Geophys Res Lett*, 2017, 44: 2725–2732
- 72 Aochi H, Fukuyama E, Matsu'ura M. Spontaneous rupture propagation on a non-planar fault in 3-D elastic medium. *Pure Appl Geophys*, 2000, 157: 2003–2027
- 73 Kase Y, Day S M. Spontaneous rupture processes on a bending fault. *Geophys Res Lett*, 2006, 33: L10302
- 74 Aochi H, Fukuyama E, Matsu'ura M. Selectivity of spontaneous rupture propagation on a branched fault. *Geophys Res Lett*, 2000, 27: 3635–3638
- 75 Bhat H S, Olives M, Dmowska R, et al. Role of fault branches in earthquake rupture dynamics. *J Geophys Res*, 2007, 112: B11309

- 76 Bai K, Ampuero J P. Effect of seismogenic depth and background stress on physical limits of earthquake rupture across fault step overs. *J Geophys Res Solid Earth*, 2017, 122: 10280–10298
- 77 Harris R A, Day S M. Dynamic 3D simulations of earthquakes on En Echelon Faults. *Geophys Res Lett*, 1999, 26: 2089–2092
- 78 Harris R A, Day S M. Dynamics of fault interaction: Parallel strike-slip faults. *J Geophys Res*, 1993, 98: 4461–4472
- 79 Hu F, Xu J, Zhang Z, et al. Supershear transition mechanism induced by step over geometry. *J Geophys Res Solid Earth*, 2016, 121: 8738–8749
- 80 Chen X. Investigations of fault friction parameters and rupture characteristics on finite seismogenic faults. Doctor Dissertation. Hong Kong: The Chinese University of Hong Kong, 2021
- 81 Somerville P G, Smith N F, Graves R W, et al. Modification of empirical strong ground motion attenuation relations to include the amplitude and duration effects of rupture directivity. *Seismol Res Lett*, 1997, 68: 199–222
- 82 Zhang Z, Zhang W, Chen X. Dynamic rupture simulations of the 2008  $M_w$  7.9 Wenchuan earthquake by the curved grid finite-difference method. *J Geophys Res Solid Earth*, 2019, 124: 10565–10582
- 83 Yang H, Yao S, He B, et al. Deriving rupture scenarios from interseismic locking distributions along the subduction megathrust. *J Geophys Res Solid Earth*, 2019, 124: 10376–10392
- 84 Shao X, Yao H, Liu Y, et al. Shallow crustal velocity structures revealed by active source tomography and fault activities of the Mianning-Xichang segment of the Anninghe fault zone, SW China. *Earth Planet Phys*, 2022, 6: 204–212
- 85 Kato A, Sakai S, Matsumoto S, et al. Conjugate faulting and structural complexity on the young fault system associated with the 2000 Tottori earthquake. *Commun Earth Environ*, 2012, 2: 13
- 86 Jiang X, Hu S, Yang H. Depth extent and  $V_p/V_s$  ratio of the Chenghai fault zone, Yunnan, China constrained from dense-array-based teleseismic receiver functions. *J Geophys Res-Solid Earth*, 2021, 126: e22190
- 87 She Y, Yao H, Yang H, et al. Constraining the depth extent of low-velocity zone along the Chenghai Fault by dense array ambient noise interferometry and horizontal-to-vertical spectral ratio. *Tectonophysics*, 2022, 827: 229265
- 88 Di Toro G, Han R, Hirose T, et al. Fault lubrication during earthquakes. *Nature*, 2011, 471: 494–498
- 89 Weng H, Yang H. Constraining frictional properties on fault by dynamic rupture simulations and near-field observations. *J Geophys Res*, 2018, 123: 6658–6670
- 90 Yao S, Yang H. Rupture dynamics of the 2012 Nicoya  $M_w$  7.6 earthquake: Evidence for low strength on the megathrust. *Geophys Res Lett*, 2020, 47: e2020GL087508
- 91 Hok S, Fukuyama E, Hashimoto C. Dynamic rupture scenarios of anticipated Nankai-Tonankai earthquakes, Southwest Japan. *J Geophys Res*, 2011, 116: B12319
- 92 Noda A, Saito T, Fukuyama E, et al. Energy-based scenarios for great thrust-type earthquakes in the Nankai trough subduction zone, Southwest Japan, using an interseismic slip-deficit model. *J Geophys Res-Solid Earth*, 2021, 126: 20
- 93 Chen X, Yang H, Jin M. Inferring critical slip-weakening distance from near-fault accelerogram of the 2014  $M_w$  6.2 Ludian earthquake. *Seismol Res Lett*, 2021, 92: 3416–3427
- 94 Atkinson G M, Boore D M. Ground-motion relations for eastern North America. *Bull Seismol Soc Am*, 1995, 85: 17–30
- 95 Boore D M, Atkinson G M. Ground-motion prediction equations for the average horizontal component of PGA, PGV, and 5%-damped PSA at spectral periods between 0.01 s and 10.0 s. *Earthq Spectra*, 2008, 24: 99–138
- 96 Somerville P G. Engineering characterization of near fault ground motion. In: 2005 New Zealand Society for Earthquake Engineering Conference. 2006, <https://www.researchgate.net/publication/237522275>
- 97 Pitarka A, Dalguer L A, Somerville D G, et al. Numerical study of ground-motion differences between buried-rupturing and surface-rupturing earthquakes. *Bull Seismol Soc Am*, 2009, 99: 1521–1537
- 98 Olsen K B, Day S M, Minster J B, et al. Strong shaking in Los Angeles expected from southern San Andreas earthquake. *Geophys Res Lett*, 2006, 33: L07305
- 99 Bydlon S A, Withers K B, Dunham E M. Combining dynamic rupture simulations with ground-motion data to characterize seismic hazard from  $M_w$  3 to 5.8 earthquakes in Oklahoma and Kansas. *Bull Seismol Soc Am*, 2019, 109: 652–671
- 100 Lachenbruch A H, Sass J H. Heat flow and energetics of the San Andreas fault zone. *J Geophys Res*, 1980, 85: 6185–6222
- 101 Gao X, Wang K. Strength of stick-slip and creeping subduction megathrusts from heat flow observations. *Science*, 2014, 345: 1038–1041
- 102 Brodsky E E, van der Elst N J. The uses of dynamic earthquake triggering. *Annu Rev Earth Planet Sci*, 2014, 42: 317–339
- 103 Yun N, Zhou S, Yang H, et al. Automated detection of dynamic earthquake triggering by the high-frequency power integral ratio. *Geophys Res Lett*, 2019, 46: 12977–12985
- 104 Yang J Q, Li Y X, Yun N D, et al. Dynamic earthquake triggering in the north of Xiaojiang fault zone, Yunnan (in Chinese). *Chin J Geophys*, 2021, 64: 3207–3219 [杨晶琼, 李月芯, 运乃丹, 等. 云南小江断裂带北段动态触发现象研究. *地球物理学报*, 2021, 64: 3207–3219]
- 105 Peng G, Lei X, Wang G, et al. Precursory tidal triggering and  $b$  value variation before the 2011  $M$  5.1 and 5.0 Tengchong, China earthquakes.

[Earth Planet Sci Lett](#), 2021, 574: 117167

- 106 Jiang X, Yang H, Yang W, et al. Crustal structure in the Binchuan basin of Yunnan constrained from receiver functions on a 2-D seismic dense array. [Earthq Sci](#), 2020, 33: 264–272
- 107 Wang B S, Zeng X F, Song Z H, et al. Seismic observation and subsurface imaging using an urban telecommunication optic-fiber cable (in Chinese). [Chin Sci Bull](#), 2021, 66: 2590–2595 [王宝善, 曾祥方, 宋政宏, 等. 利用城市通信光缆进行地震观测和地下结构探测. 科学通报, 2021, 66: 2590–2595]
- 108 Zhou Y S, He C R. Rheological parameters of crustal rocks and crustal rheology of North China (in Chinese). [Seismol Geol](#), 2003, 23: 109–122 [周永胜, 何昌荣. 地壳主要岩石流变参数及华北地壳流变性质研究. 地震地质, 2003, 23: 109–122]
- 109 Zhou Y S, He C R. The rheological structures of crust and mechanics of high-angle reverse fault slip for the Wenchuan  $M_s$  8.0 earthquake (in Chinese). [Chin J Geophys](#), 2009, 52: 474–484 [周永胜, 何昌荣. 汶川地震区的流变结构与发震高角度逆断层滑动的力学条件. 地球物理学报, 2009, 52: 474–484]

Summary for “非均匀断层上的破裂传播及对震级预测的挑战”

# Rupture propagation on heterogeneous fault: Challenges for predicting earthquake magnitude

Hongfeng Yang<sup>1,2\*</sup>, Suli Yao<sup>1</sup> & Xiang Chen<sup>1</sup>

<sup>1</sup> Earth System Science Programme, the Chinese University of Hong Kong, Hong Kong, China;

<sup>2</sup> Shenzhen Research Institute, the Chinese University of Hong Kong, Shenzhen 518057, China

\* Corresponding author, E-mail: [hyang@cuhk.edu.hk](mailto:hyang@cuhk.edu.hk)

Predicting magnitudes and ground motion of future strong earthquakes on seismogenic faults holds critical implications on seismic hazard zonation and mitigation. Although present approaches on seismic hazard assessment can effectively identify potential regions to host strong earthquakes, it remains extremely challenging to accurately predict future earthquake magnitudes because of various heterogeneities of fault zones, such as fault geometry, medium structure, and frictional properties. In this work, we review a few aspects that play important roles in earthquake rupture propagation and extent, so as to determine the final magnitude of earthquakes.

Under the condition of heterogeneous stress distribution on faults, the final magnitude of earthquakes as well as shallow slip distribution depends on where the rupture initiates. As shown in recent numerical models of dynamic rupture simulations, different hypocenters with similar stress level can lead to completely different rupture scenarios, some of which may significantly break the ground whereas others may be buried underground. Such findings shed critical lights on seismic hazard preparation, because surface-breaching ruptures can lead to severe damage as vividly evidenced by the 2022 Menyuan  $M_w$  6.7 earthquake. To date, we cannot predict future hypocenter locations according to our knowledge of earthquake nucleation and therefore future relevant investigations are highly demanded.

Furthermore, the size of seismogenic zone on strike-slip faults controls whether ruptures may become “break-away” to form large earthquakes or stop spontaneously as “self-arresting” of moderate magnitude events. Observations show that aspect ratios between rupture length and down-dip width of dip-slip earthquakes are usually no more than 8. In contrast, the length/width ratios of strike-slip earthquakes may rise to 40 and have a drastic change around the rupture width of ~10 km. Intrinsic mechanism of such variation in strike-slip earthquakes is attributed to the energy release rate of rupture fronts, which is controlled by the down-dip width. As such, high-resolution constraints on down-dip seismogenic width can be used to estimate the magnitude of future earthquakes on strike-slip faults.

Moreover, fault zone structure significantly affects rupture directivity and slip extents. For instance, low velocity fault zones may promote rupture propagation and thus enlarge the earthquake magnitude. Given the rapid development of seismic observations and seismic imaging techniques, high-resolution fault zone structure can be obtained from data recorded by dense arrays, including nodal network and the newly developed distributed acoustic sensing (DAS) arrays. Integrating with laboratory results of rheology from samples representing crustal rocks, the near-fault high-resolution seismic structure can be converted into rheological properties on faults, which can then be used to outline asperities for future earthquakes. This may provide a critical step to link seismic structure to earthquake potential, as the outlined asperities can be further used to derive rupture scenarios and earthquake magnitudes.

To advance our understanding on this front, future work may integrate multiple sources of observations and modeling. Conducting rupture simulations with constraints from geodetic and seismic measurements, as well as laboratory frictional experiments, can be helpful in exploring potential earthquake magnitudes. By considering heterogeneities on faults with reasonable constraints, the numerical models can be useful of investigating the probable hypocenter locations of large earthquakes. Thus, the numerical results may support future near-field observations to improve monitoring of nucleation and development of future large earthquakes. Furthermore, the ground motions generated from the numerical models can also fill the data gap of near-field observations of large earthquakes and provide critical support for physics-based seismic hazard assessment.

**earthquake prediction, fault zone heterogeneities, earthquake rupture propagation, hypocenter-dependent effect, dynamic rupture simulations**

doi: [10.1360/TB-2021-1086](https://doi.org/10.1360/TB-2021-1086)